1 **Tracing subducted oceanic slabs in the mantle by**

2 **using molybdenum isotopes: A case study of**

3 **intraplate basalts from the Northeast China**

5 Qiugen Zheng[A], Qifang Zheng[B]*, Yi Zhang[C]*, Guangyu He [D], Qian Wang[D], Jane Fitton[E]

6 A.School of Ocean Sciences, China University of Geosciences (Beijing), Beijing,

7 China,100083

8 B. School of Earth Sciences and Resources, China University of Geosciences (Beijing),

9 Beijing, China,100083

10 C.School of Earth Sciences, ZheJiang University, Hangzhou, China, 310058

11 D. State Key Laboratory of Isotope Geochemistry, Guangzhou Institute of Geochemistry,

12 Chinese Academy of Sciences, Guangzhou, China, 510630

13 E. Dept of Earth Sciences, University of Oxford, South Parks Road, Oxford OX1 3AN, UK

16 * Corresponding author:

17 Qifang Zheng and Yi Zhang

18 E-mail: xiaoyi_tu2021@163.com

19   zhangyi920407@163.com

22

23 **Abstract**

24 Determining subducted processes is very important for understanding lithological

25 heterogeneity because substantial quantities of slabs are recycled into the mantle. Molybdenum

26 isotopes have been used to distinguish sources materials because of the significant Mo isotopic

27 differences between the crust and the mantle. Here, we undertake a systematic Mo isotopic

28 investigation on a suite of well-characterized continental basalts from Keluo and Halaha-

29 Chaoer, located in Northeast China. δ^{98}Mo of Keluo varied from -0.41 to -0.23‰ with an

30 average of -0.34‰, and samples from Halaha-Chaoer ranged in δ^{98}Mo from -0.18 to -0.12‰

31 with an average of -0.15‰. The former is lighter than the mean value of fresh oceanic basalts

32 (-0.21‰), while the latter is similar to oceanic basalts. Combined with other geochemical

33 indications (LOI, Ce/Pb, La/Yb and so on), the Mo isotopic variations cannot be interrupted by

34 chemical weathering, continental crust contamination, or magmatic processes. The δ^{98}Mo

35 variation in this study is explained by adding various oceanic crustal materials in magma

36 sources. The relationships of δ^{98}Mo with Ba/Th, Th/U, ^{143}Nd/^{144}Nd for the samples indicated

37 that sediment and altered oceanic crust have contributed to the significant variations in these

38 samples. This study indicates the great potential of Mo isotopes to distinguish different types

39 of recycled oceanic crust materials in the mantle.

40

41

42 Keywords: Molybdenum isotopes; Subducted oceanic slabs; Intraplate basalts; Northeast China

43

1. Introduction

Slab subduction is widely considered to be the primary mechanism for element cycling between the crust and mantle (Hofmann, 1997; Stracke et al., 2003). The recycled materials with slabs subduction are used to either generate the magmas in the subduction zone or form different reservoirs, such as enriched mantle component I (EM I) and enriched mantle component II (EM II) (Zindler and Hart, 1986). Previous investigations suggested that the oceanic crust account for ~10% of the total mass of the mantle since the starting of subducted processes (Stracke et al., 2003; Tang et al., 2016). The converted approach took varied materials into mantle and led to lithological heterogeneity in the upper mantle (Perfit et al., 1980; Plank and Langmuir, 1998; Castillo et al., 2000). Therefore, distinguishing the contribution of subducted materials was required for understanding the lithological heterogeneity.

The previous works observed that the mobility of Mo could be negligible in the subduction zones (Noll et al., 1996; Bali et al., 2012), suggesting that Mo isotopic composition of subdued material can be recorded in the mantle (Freymuth et al., 2015). Supposing there are significant differences in δ^{98}Mo and Mo concentration between the upper mantle, fresh oceanic crust, altered oceanic crust, and sediment, the Mo isotope system will be a powerful tool to trace the sources of magma and calculate the contribution proportion of each source. Bezard et al. (2016) measured the Mo isotopic composition of Mid-Ocean Ridges Basalt (MORB) to establish the Mo isotopic composition of the depleted mantle (DM) as -0.21±0.02‰. Freymuth et al. (2015) analyzed the sediment and altered oceanic crust from ODP sites 801 and 802, ranging in δ^{98}Mo from -1.87 to 0.11‰ with an average value of -0.50‰ and from -0.88 to 0.86‰ with an average value of -0.03‰, respectively. Moreover, the Mo concentrations of the upper mantle, altered oceanic crust, and sediment are 1.65 μg g^{-1}, 0.35 μg g^{-1}, and 4.03 μg g^{-1}, respectively. The significant differences in Mo isotopic composition and Mo concentrations between mantle and crust indicate that Mo isotope has excellent potential to trace subducted processes.

Due to the natural advantage of the Mo isotope, many investigations focused on oceanic basalt using Mo isotopic system to trace the subducted processes (König et al., 2016; Willbold and Elliott, 2017; Zhang et al., 2020; Li et al., 2021). However, the current Mo isotope data of intraplate basalt is very limited, and it is debated for using Mo isotope to trace recycled

73 materials for intraplate basalt. Here, we measured a systematic Mo isotopic composition of a

74 set of well-characterized basalt samples from Keluo and Halaha-Chaoer of Northeast China.

75 Samples from Keluo display typical EM I characteristics, while samples from Halaha-Chaoer

76 have the radiogenic isotopic signatures of the focal zone (FOZO) (Hart et al., 1992; Stracke et

77 al., 2005). Thus, the samples allow us to use the Mo isotope to assess the contributions of

78 recycled crustal materials to the mantle.

79 **2 Sample**

80 Northeast China was set between the Siberian Craton and the North China Craton, and

81 considered as the eastern segment of the Central Asian Orogenic Belt (Chen et al., 2007; Zhang

82 et al., 1995). The plate suffered the closure of the Paleo-Asian Ocean and the amalgamation of

83 many microcontinent (Senger et al., 1993). Intraplate basaltic rocks in North China were formed

84 in the Cenozoic (Zhang et al., 1995; Zou et al., 2003). The Halaha-Chaoer and Keluo volcanic

85 fields were set at the Great Xing'an Mountains and the North of Songliao Basin (Zhang, 1992).

86 Fourteen samples were collected from two volcanic fields, including Halaha-Chaoer (2.0 Ma)

87 and Keluo (9.6–0.11 Ma), of Northeast China. These samples come from many works which

88 studied the evolution of volcanoes. Therefore, the geochemical and isotopic compositions of

89 more samples can be found in previous works (Sun et al., 2014, 2017), and particle samples are

90 measured in this study (Table S1). Here, we just provided a brief description of these samples.

91 The Mo concentration and MgO content of Halaha-Chaoer lavas ranged from 0.96 to 1.18 μg

92 g^{-1} with an average value of 1.05 ± 0.18 μg g^{-1} and from 7.93 to 12.13 wt. %, suggesting

93 significant crystallization. And the Sr-Nd isotopic ratios of Halaha-Chaoer samples is similar

94 to the FOZO component (initial $^{87}Sr/^{86}Sr$ = 0.70354 - 0.7037 and $^{143}Nd/^{144}Nd$ = 0.51291 -

95 0.5193). On the contrary, the Keluo lavas are characterized by a high Mo concentration of 1.21-

96 2.63 μg g^{-1} and same MgO content (7.67 to 11.28 wt.%) in relation to Halaha-Chaoer lavas. The

97 Sr-Nd isotopic compositions of the group sample are close to the EMI component ($^{87}Sr/^{86}Sr$ =

98 0.70503–0.70541 and $^{143}Nd/^{144}Nd$ = 0.51235–0.51246) (Table 1). The significant chemical

99 difference between Keluo and Halaha-Chaoer provided a great opportunity to check the ability

100 of Mo isotope to trace the contributions of recycled crustal materials to the mantle.

101 **3 Analytical methods**

102 3.1 Major and trace element analyses

103 The major and trace elements were conducted following the analytical procedures described by

104 Qi et al. (2000). An Inductively Coupled Plasma-Atomic Emission Spectrometer measured the

105 major elemental compositions. The loess on ignition (LOI) was analyzed after the samples were

106 heated for 30 min at 980℃. The samples were digested using a mixture of HF-HNO$_3$-HF. The

107 clean solutions were diluted to determine the trace element composition on an Inductively

108 Coupled Plasma-Mass Spectrometry (ELEMENT XR, Thermo, Germany). The reproducibility

109 for trace elements is better than 10% (2SD). All uncertainties of the major element are better

110 than 2% (2SE).

111 3.3 Mo-Sr-Nd isotopic analyses

112 The Mo isotopic measurement of all samples was carried out at the State Key Laboratory of

113 Isotope Geochemistry, Guangzhou Institute of Geochemistry, Chinese Academy of Sciences.

114 Detailed processes for digestion, chemical purification and isotopic analysis can be found in Li

115 et al. (2014) and Zhao et al. (2017). Sr-Nd isotopes were determined at the China University of

116 Geosciences, Beijing, and a more ~~analyzed method~~ can be found in Xu et al. (2021).

117 The samples were digested using a 7 ml PFA beaker. Approximately 50-100 mg of powdered

118 samples were mixed with 2ml of concentrated HF and 1 ml of concentrated HNO3; the mixtures

119 were heated at 185±5℃ for 36 h. The dry residues were dissolved into Aqua regia to digest

120 samples completely. The fully dissolved samples were evaporated to dryness and then

121 redissolved in 5ml 1.5 M HNO3.

122 The digested samples containing 100-200 ng Mo were spiked by ~~the~~ double spikes (^{100}Mo-^{97}Mo)

123 in a 15ml PFA beaker to correct ~~the~~ potential Mo isotopic fractionation of chemical purification

124 and measurement. The spiked samples were dried slowly at 90℃ to allow the equilibration

125 between the samples and double spike and then redissolved in 4ml ~~mixed acid~~ of 0.1 M HF and

126 1M HCl. The sample solutions were loaded ~~to~~ prepare BPHA resin that was clean with 6 M

127 HCl and MQ. The matrix elements were washed out of columns by 0.1M HF-1M HCl. The

128 fraction of Mo was collected by 6 M HF-1M HCl in a 15ml PFA beaker. The eluted solutions

129 were evaporated to dry at 130℃. Concentrated HNO3 and H$_2$O$_2$ were used to remove residual

130 organic materials from the resin. The total bank of the procedure is 0.5ng which can be

131 neglected in relation to the loaded sample. Sr and Nd were purified from matrix elements using

132 AG50W-X12 (200-400 mesh) resin and LN resin, respectively.

133 Molybdenum isotopic measurements were performed with a Multi-collector inductively

134 coupled plasma mass spectrometer (MC-ICP-MS, Neptune Plus, ThermoFisher). Sample

135 solutions were introduced into the plasma by an Aridus II desolvator system. The signal

136 sensitivity of ^{95}Mo was $\geq$ 190 V μg^{-1} mL, and the bank signal of ^{95}Mo was less than 4 mV. The

137 solutions and samples were dissolved at 0.5 M HHNO$_3$ and diluted to 30 ng mL^{-1} for measuring

138 Mo isotopes. All Mo isotope analyses were carried out on the low mass resolution mode

139 (ΔM/M<3000). The on-peak instrument and acid matrix blank were determined by measuring

140 1.5M HNO$_3$ before each sample and standard to subtract from the signal intensities. Every 5

141 samples were bracketed by a spiked SRM 3134 with 30 ng mL^{-1} to normalize the Mo isotope

142 ratio of samples. More detailed parameters for the Mo isotopes measurements have been listed

143 in previous work. The Mo isotopic composition is expressed relative to NIST SRM 3134 as

144 delta (δ) notation: δ^{98}Mo=((^{98}Mo/^{95}Mo) $_{sample}$/(^{98}Mo/^{95}Mo)$_{NIST\ SRM\ 3134}$-1) × 1000. Four

145 geological reference materials (NOD-A-1, NOD-P-1, BHVO-2 and BCR-2) from USGS were

146 digested, purified and measured with our samples. The Mo isotopic compositions re -0.79±0.04‰

147 (2SD, n=5) for NOD-A-1, -0.87±0.05‰ (2SD, n=5) for NOD-P-1, -0.05±0.05‰ (2SD, n=5)

148 for BHVO-2 and -0.06±0.04‰ (2SD, n=5) for BCR-2, similar to previous works (Skierszkan

149 et al., 2015; Li et al., 2016; Willbold et al., 2016).

150 For Sr and Nd isotopic composition, the mass fractionations of chemical purification and

151 instrument were calibrated with ^{88}Sr/^{86}Sr=8.375209 and ^{146}Nd/^{144}Nd=0.7219. The long-term

152 analysis gave 0.710241 ± 24 for ^{87}Sr/^{86}Sr of NIST SRM 987 in the lab and 0.512434 ± 29 for

153 ^{143}Nd/^{144}Nd of Alfa Aesar Nd. The Sr and Nd isotopic composition of BHVO-2 and BCR-2

154 determined in this study are consistent with previous values (Li et al., 2012).

155 **4. Results**

156 The δ^{95}Mo values of Northeast China lavas vary from -0.41‰ to -0.12‰ (Table 1). The sample

157 from Keluo varied from -0.41 to -0.23‰ in δ^{95}Mo with an average of -0.34±0.10‰ (2SD),

158 higher than the sediments (-0.50‰) and lighter than the altered oceanic basalts (0.03‰)

159 (Freymuth et al., 2015). The samples from Halaha-chaoer have homogenous Mo isotopic

160   composition, ~~ranging~~ from -0.12 to -0.18‰ with an average of -0.15±0.05‰ (2SD), similar to

161   the fresh MORB (-0.21‰, Chen et al., 2022). The Sr-Nd isotopes, major and trace elements

162   composition ~~were shown~~ in Table 1 and Table S1.

163   **5. Discussion**

164   Given Mo isotope can be fractionated during a range of processes, it is necessary to carefully

165   assess the processes that may have modified Mo isotopic composition of these samples, such

166   as chemical weathering, assimilation of shallow continental crust, magmatic differentiation and

167   partial melting. ~~And then, we~~ estimate the effects of recycled crustal materials on the Mo

168   isotopic variation of the samples.

169   **5.1 Chemical weathering and Assimilation of crustal materials on Mo isotope**

170   Mo isotopes ~~were~~ fractionated during chemical weathering, and lighter isotopes adsorbed onto

171   secondary minerals so that the weathered residual is lighter in δ^{95}Mo than fresh igneous rocks

172   (Greaney et al., 2021). However, the samples do not observe secondary minerals (Sun et al.,

173   2014). Moreover, the loss on ignition (LOI) ranging from 0.00 to 1.28 does not display a

174   negative correlation (Fig. 1). Both pieces of evidences imply that the observed Mo isotopic

175   variation cannot be attributed to chemical weathering.

176   These basalts erupted through the continental crust, which is about 40km. The Mo content of

177   these basalts varies from 1.28 to 2.82 μg g^{-1} with an average value of 1.83 μg g^{-1}, higher than

178   the average Mo concentration of continental crust is 0.8 μg g^{-1} (Rudnick and Gao, 2014). The

179   upper continental crust is significantly different in δ^{95}Mo from the basalt (Yang et al., 2017;

180   Greaney et al., 2020). Hence, we must consider that crustal materials may modify the Mo

181   isotopic composition of these basalts. For the scenario, a negative correlation between Mo

182   content and δ^{95}Mo were expected because of the heavy Mo isotopic composition of the

183   continental crust. However, we do not observe the relationship (Fig. 2). On the other hand,

184   binary mixing calculation implies that the Mo isotopic variation cannot be explain by binary

185   mixing between continental crust and mantle melt, because of unrealistic Mo concentration

186   ratio (Fig. 2). Hence, Assimilation of crustal materials is not the main process that leaded to the

187   Mo isotopic variation in these basalts.

188

5.2 The effect of fractional crystallization on Mo isotope

189

190 The Mo isotopic composition of basalts from the Kos Island arc system ranged from 0.3 to

191 0.6‰, indicating that Mo isotopes are fractionated during the fractional crystallization of

192 hornblende and biotite (Voegelin et al., 2014). However, Bezard et al. (2016) measured the Mo

193 isotopic composition of MORB from the Pacific-Antarctic ridge and the Mohns-Knipovich

194 ridge. The δ^{95}Mo did not show correlations with MgO that indicated magma differentiation,

195 suggesting that Mo isotopic fractionation is insignificant during the fractional crystallization of

196 MORB magma. Recently, Chen et al. (2022) analyzed some MORB glass to constrain the Mo

197 isotopic composition of the upper mantle. The correlations between δ^{95}Mo and magmatic

198 differentiation indicators were not observed, inferring that Mo isotopes were not fractionated

199 during magmatic differentiation (Chen et al., 2022). For our samples studied here, the

200 significant variation of MgO contents (from 6.9 to 13.0%) implies that fractional crystallization

201 plays an essential role in changing the chemical composition of basalts. As shown in Fig.3a,

202 Mo concentration in basalt from Northeast China correlates well with MgO; the positive

203 correlation indicates that Mo is a likely incompatible element enriched in solid phases during

204 melt evolution. The unclear correlations between δ^{98}Mo and MgO (Fig. 3b) and Mo (Fig. 2)

205 content suggest that the effect of fractional crystallization on the δ^{95}Mo of basalts is likely

206 insignificant. The observation is similar to the previous inference (Bezard et al., 2016 and Chen

207 et al., 2022) but different from the conclusions from Voegelin et al. (2014). Thus, the δ^{98}Mo

208 variation cannot be explained simply to fractional crystallization and may be caused by partial

209 melting.

5.3 The effect of partial melting on Mo isotopic composition of basalts

210

211 Since sodium is a moderately incompatible element at melting the with highest concentration

212 at started melting, the Na concentration of melt decreases with the growth of melting degree.

213 Hence, Na$_{8.0}$ indicates the degree of partial melting without the effect of fractional

214 crystallization (Klein and Langmuir, 1987). Bezard et al. (2016) observed the absence of

215 correlation between δ^{95}Mo and Na$_{8.0}$, explaining the trend that Mo isotopes are not fractionated

216 during mantle melting. Since La is more incompatible than the heavy rare earth element Yb

217 during the partial melting of mantle, (La/Yb)$_N$ ratio is sensitive to the degree of partial melting.

218   Liang et al. (2017) observe broad correlations between δ^{98}Mo and (La/Yb)$_N$ in ocean island

219   basalts (OIB), suggesting a significant effect of melting on the Mo isotopic variations. The

220   conclusion is contrary to Bezard et al. (2016). However, for our samples, we did not observe

221   the clear relationships between δ^{98}Mo and Na$_{8.0}$ (Fig. 4a) as well as (La/Yb)$_N$ (Fig. 4b). In

222   addition, McCoy-West et al. (2019) accessed the Mo isotopic behaviors using a non-modal

223   batch melting model and inferred that Mo isotopes were significantly fractionated during

224   mantle partial melting that melt is heavier in δ^{98}Mo than the residue. The fractionation was

225   driven from as that Mo (VI) with heavier isotope is more incompatible than Mo (IV) (Leitzke

226   et al., 2017). However, the samples (-0.33±0.10‰) produced by the high degree of partial

227   melting have lighter Mo isotopic composition than the samples with a low degree (-

228   0.15±0.05‰), contrary to the prediction trend by the previous model (Fig. 4, McCoy-West et

229   al., 2019). Therefore, the evidences suggested that partial melting cannot explain the δ^{98}Mo

230   variation of these basalts.

231   **5.4 Molybdenum isotopic variation induced by crustal recycling**

232   The above discussions show that the Mo isotopic variation for these basalts cannot be explained

233   by shallow-level processes, fractional crystallization and partial melting. Radiogenic isotopes,

234   such as Nd and Sr, usually are used to reflect heterogeneous sources. The significant variations

235   for ^{143}Nd/^{144}Nd and δ^{98}Mo imply that there are more than two components at least for the mantle

236   sources of these basalts (Fig. 5). In the following, we will discuss the mechanisms that may be

237   responsible for the processes of mantle enrichment and ~~abnormal~~ Mo isotopic ~~composition.~~

238

239   Sediments could be recycled into the mantle with subducted slabs (Stracke et al., 2003). The

240   δ^{98}Mo of subducting sediments ~~varied~~ from -1.87 to 0.11‰ with an average value of -0.50 ±

241   0.27‰ (2SE, n=16, Freymuth et al., 2015). Since Mo is a highly incompatible element and

242   lighter isotopes were preserved in the residual ~~produced~~ during metamorphic dehydration

243   (König et al., 2016), melts derived from recycled sediments should inherit the light Mo isotopic

244   composition. Hence, the incorporation of recycled sediments into peridotite melting could be

245   responsible the lighter Mo isotopic composition. The δ^{98}Mo of basalt studied here (-0.30‰) is

246   lighter than fresh MORB (-0.21‰, Chen et al., 2022), and ^{143}Nd/^{144}Nd is higher than sediment

247   (0.51228, Vervoort et al., 2011) and lighter than fresh MORB (0.513074, Gale et al., 2013),

248   suggesting that sediment is one of source for these basalts from Keluo. On the other hand, Th/U

249   ratio is not fractionated significantly during magmatic processes as Th and U are incompatible

250   elements. Both elements can be fractionated during fluid processes because of the higher

251   mobility of U than Th (Hawkesworth et al., 1997; Bali et al., 2009; Ling et al., 2011). Thus,

252   there is a significant difference in the Th/U ratio between fresh MORB (3.54, Gale et al., 2013)

253   and sediment (6.64, Vervoort et al., 2011). Reasonability, the ratio is usually used as an indicator

254   of distinguishing the mantle sources (Sun et al., 2020). The Th/U ratio of our basalts (4.94 to

255   6.12) falls between sediment and fresh MORB. The observation indicates that sediment may

256   play an essential role in forming these basalts. It is noteworthy that there is not expected positive

257   correlation between $\delta^{98}Mo$ and Th/U ratio (Fig. 5b), implying other sources for the basalts.

258   Significant Mo isotopic fractionation is observed during seawater alteration (Freymuth et al.,

259   2015), suggesting that altered oceanic crust (-0.02‰) is heavier $\delta^{98}Mo$ than fresh ocean crust

260   (-0.21‰). Thus, The incorporation of altered oceanic crust during the particle melting of mantle

261   could produce melts with ~~significant~~ ~~various~~ Mo isotopic composition. Due to the mobility

262   difference between Ba and Th (Weaver et al., 1986), the Ba/Th ratio of the altered oceanic crust

263   will be increased with the growing extent of low-temperature hydrothermal alteration (Kelley

264   et al., 2003). Furthermore, the ratio will not be changed during slab dehydration (Kogiso et al.,

265   1997; Kessel et al., 2005). Hence, the ratio is used to trace the incorporation of altered oceanic

266   crust in the mantle (Sun et al., 2020). The Ba/Th ratios of these basalts range from 147 to 239,

267   higher than sediment and fresh MORB and similar to altered oceanic crust (Fig. 5c), indicating

268   the incorporation of altered oceanic crust into the source region of these basalts.

269   Therefore, recycled sediment and altered both have contributed to the basalt of Keluo produced

270   in Northeast China. The materials may have come from the westward subduction of the Pacific

271   plate (Tang et al., 2014). The contribution of the fresh oceanic crust is insignificant because of

272   the low Mo concentration. Mixing of melts produced from recycled sediment with the

273   contribution of mantle peridotites derived the variation of Mo isotopic composition in the

274   basalts.

275   **6. Conclusion**

276   This work suggests that the basalt from Keluo displays heterogenous Mo isotopic composition

277   and is heavier Mo isotopic compositions than the upper mantle. At the same time, the sample

278   from Halaha-Chaoer is homogenous in δ^{98}Mo, similar to the upper mantle. The isotopic

279   variation was explained by adding sediment and altered oceanic basalt with subducted oceanic

280   slabs into mantle sources. Therefore, the Mo isotope is a powerful tool in investigating the

281   effect of crustal recycling on mantle-derived magmas to understand recycling materials' roles

282   in mantle heterogeneity.

283

284   **Acknowledgements**

285   We are grateful to Jie Li and FanHuang Li for analytical assistance, as well as Yang Sun and

286   Yongwei Zhao for sample collection. The work was supported by the National Key Research

287   and Development Program of China (2017YFC0703201), the National Science and Technology

288   Major Project of the Ministry of Science and Technology of China (2016ZX05014001), the

289   Strategic Priority Research Program of the Chinese Academy of Sciences (XDA14010201), the

290   National Natural Science Foundation of China (41530347, 41872225)

291   **Reference**

292   Bali E., Audetat A. and Keppler H. (2009) Mobility of U and Th in subduction zone fluids-A

293   synthetic fluid inclusion study. Geochim. Cosmochim. Acta 73(13), A80.

294   Bali, E., Keppler, H., Audetat, A., 2012. The mobility of W and Mo in subduction zone fluids and

295   the Mo–W–Th–U systematics of island arc magmas. Earth Planet. Sci. Lett. 351–352, 195–

296   207.

297   Bezard R., Fischer-Godde M., Hamelin C., Brennecka G. A. and Kleine T. (2016) The effects of

298   magmatic processes and crustal recycling on the molybdenum stable isotopic composition of

299   Mid-Ocean Ridge Basalts. Earth Planet. Sci. Lett. 453, 171–181.

300   C.J. Hawkesworth, S.P. Turner, F. McDermott, D.W. Peate, P. van Calsteren, U-Th isotopes in arc

301   magmas implications for element transfer from the subducted crust, Science 276 (1997) 551-

302   555.

303   Castillo P. R. (2015) The recycling of marine carbonates and sources of HIMU and FOZO ocean

304   island basalts. Lithos 216–217, 254–263.

305 Chen, S., Sun, P., Niu, Y., Guo, P., Elliott, T., Hin, R.C., 2022. Molybdenum isotope systematics of

306 lavas from the East Pacific Rise: constraints on the source of enriched mid-ocean ridge basalt.

307 Earth Planet. Sci. Lett. 578, 117283.

308 Commun. 12, 6015.

309 Freymuth H., Vils F., Willbold M., Taylor R. N. and Elliott T. (2015) Molybdenum mobility and

310 isotopic fractionation during subduction at the Mariana arc. Earth Planet. Sci. Lett. 432, 176–

311 186.

312 Gale A., Dalton C. A., Langmuir C. H., Su Y. and Schilling J.-G. (2013) The mean composition of

313 ocean ridge basalts. Geochem. Geophys. Geosyst. 14, 489–518.

314 Greaney, A.T., Rudnick, R.L., Romaniello, S.J., Johnson, A.C., Gaschnig, R.M., Anbar, A.D., 2020.

315 Molybdenum isotope fractionation in glacial diamictites tracks the onset of oxidative

316 weathering of the continental crust. Earth Planet. Sci. Lett. 534, 116083.

317 Hart S. R., Hauri E. H., Oschmann L. A. and Whitehead J. A. (1992) Mantle plumes and

318 entrainment-Isotopic evidence. Science 256, 517–520

319 Hofmann A. W. (1997) Mantle geochemistry: The message from oceanic volcanism. Nature 385,

320 219–229.

321 Kelley K. A., Plank T., Ludden J. and Staudigel H. (2003) Composition of altered oceanic crust at

322 ODP Sites 801 and 1149. Geochem. Geophys. Geosyst. 4, 8910. https://doi.org/

323 10.1029/2002GC000435

324 Kessel R., Schmidt M. W., Ulmer P. and Pettke T. (2005) Trace element signature of subduction-

325 zone fluids, melts and supercritical liquids at 120–180 km depth. Nature 437, 724–727.

326 Klein E. and Langmuir C. H. (1987) Global correlations of ocean ridge basalt chemistry with axial

327 depth and crustal thickness. J. Geophys. Res. 92, 8089–8115

328 Kogiso T., Tatsumi Y. and Nakano S. (1997) Trace element transport during dehydration processes

329 in the subducted oceanic crust: 1. Experiments and implications for the origin of ocean island

330 basalts. Earth Planet. Sci. Lett. 148, 193–205.

331 Konig S., Wille M., Voegelin A. and Schoenberg R. (2016) Molybdenum isotope systematics in

332 subduction zones. Earth Planet. Sci. Lett. 447, 95–102.

333 Leitzke F. P., Fonsecaa R. O. C., Sprungb P., Mallmannc G., Lagosa M., Michelya L. T. and Mu¨nker

334   C. (2017) Redox dependent behaviour of molybdenum during magmatic processes in the

335   terrestrial and lunar mantle: implications for the Mo/W of the bulk silicate Moon. Earth Planet.

336   Sci. Lett. 474, 503–515.

337 Li C.-F., Li X.-H., Li Q.-L., Guo J.-H., Li X.-H. and Yang Y.-H. (2012) Rapid and precise

338   determination of Sr and Nd isotopic ratios in geological samples from the same filament

339   loading by thermal ionization mass spectrometry employing a single-step separation scheme.

340   Anal. Chim. Acta 727, 54–60.

341 Li H. Y., Zhao R. P., Li J., Tamura Y., Spencer C., Stern R. J., Ryan J. G. and Xu Y. G. (2021)

342   Molybdenum isotopes unmask slab dehydration and melting beneath the Mariana arc. Nat.

343   Arc). Lithos 190–191, 440–448.

344 Li J., Liang X.R., Zhong L.F., Wang X.C., Ren Z.Y., Sun S.L., Zhang Z.F. and Xu J.F. (2014).

345   Measurement of the isotopic composition of molybdenum in geological samples by MC-ICP-

346   MS using a novel chromatographic extraction technique. Geostand. Geoanal. Res, 38, 345–

347   354,

348 Li, J., Liang, X.-R., Zhong, X.-C., Wang, Z.-Y., Ren, S.-L., Sun, Z.-F., Zhang, J.-F., Xu, J.-F., 2014.

349   Measurement of the isotopic composition of molybdenum in geological samples by MC-IC-

350   MS using a novel chromatographic extraction technique. Geostand. Geoanal. Res. 38 (3), 345–

351   354.

352 Liang Y. H., Halliday A. N., Siebert C., Fitton J. G., Burton K. W., Wang K. L. and Harvey J. (2017)

353   Molybdenum isotope fractionation in the mantle. Geochim. Cosmochim. Acta 199, 91–111.

354 Ling M. X., Wang F. Y., Ding X., Zhou J. B. and Sun W. D. (2011) Different origins of adakites

355   from the Dabie Mountains and the Lower Yangtze River Belt, eastern China: geochemical

356   constraints. Int. Geol. Rev. 53(5–6), 727–740.

357 McCoy-West A. J., Chowdhury P., Burton K. W., Sossi P., Nowell G. M., Fitton J. G., Kerr A. C.,

358   Cawood P. A. and Williams H. M. (2019) Extensive crustal extraction in Earth's early history

359   inferred from molybdenum isotopes. Nat. Geosci. 12, 946–951

360 Noll, P.D., Newsom, H.E., Leeman, W.P., Ryan, J.G., 1996. The role of hydrothermal fluids in the

361   production of subduction zone magmas: evidence from siderophile and chalcophile trace

362   elements and boron. Geochim. Cosmochim. Acta 60, 587–611.

363 Perfit, M., Gust, D., Bence, A., Arculus, R., Taylor, S.R., 1980. Chemical characteristics of island-
364   arc basalts – implications for mantle sources. Chem. Geol. 30 (3), 227–256.

365 Plank, T., Langmuir, C.H., 1998. The chemical composition of subducting sediment and its
366   consequences for the crust and mantle. Chem. Geol. 145, 325–394

367 Qi, L., Hu, J., Gregoire, D.C., 2000. Determination of trace elements in granites by inductively
368   coupled plasma–mass spectrometry. Talanta 51, 507–513.

369 Rudnick R. L. and Gao S. (2014) Composition of the continental crust. In Treatise on Geochemistry
370   (eds. H. D. Holland and K. K. Turekian), second ed. Elsevier, Oxford, pp. 1–51.

371 Skierszkan EK, Amini M, Weis D (2015) A practical guide for the design and implementation of the
372   double-spike technique for precise determination of molybdenum isotope compositions of
373   environmental samples. Anal Bioanal Chem 407:1925–1935

374 Stracke A., Bizimis M. and Salters V. J. M. (2003) Recycling oceanic crust: Quantitative constraints.
375   Geochem. Geophys. Geosyst. 4, 8003. https://doi.org/10.1029/ 2001GC000223, 3.

376 Stracke A., Hofmann A. W. and Hart S. R. (2005) FOZO, HIMU, and the rest of the mantle zoo.
377   Geochem. Geophys. Geosyst. 6, Q05007. https://doi.org/10.1029/2004GC000824.

378 Sun Y., Teng F.-Z., Ying J.-F., Su B.-X., Hu Y., Fan Q.-C. and Zhou X.-H. (2017) Magnesium
379   isotopic evidence for ancient subducted oceanic crust in LOMU-like potassium-rich volcanic
380   rocks. J. Geophys. Res. Solid Earth 122, 7562–7572.

381 Sun Y., Ying J., Zhou X., Shao J. A., Chu Z. and Su B. (2014) Geochemistry of ultrapotassic volcanic
382   rocks in Xiaogulihe NE China: implications for the role of ancient subducted sediments. Lithos
383   208–209, 53–66.

384 Tang Y., Obayashi M., Niu F., Grand S. P., Chen Y. J., Kawakatsu H., Tanaka S., Ning J. and Ni J.
385   F. (2014) Changbaishan volcanism in northeast China linked to subduction-induced mantle
386   upwelling. Nat. Geosci. 7, 470–475.

387 Vervoort J. D., Plank T. and Prytulak J. (2011) The Hf–Nd isotopic composition of marine sediments.
388   Geochim. Cosmochim. Acta 75, 5903–5926

389 Voegelin A. R., Pettke T., Greber N. D., von Niederha¨usern B. and Na¨gler T. F. (2014) Magma
390   differentiation fractionates Mo isotope ratios: evidence from the Kos Plateau Tuff (Aegean

391 Willbold M. and Elliott T. (2017) Molybdenum isotope variations in magmatic rocks. Chem. Geol.

392   449, 253–268.

393   WillboldM., Hibbert K., Lai Y. J., Freymuth H., HinR. C., Coath C., Vils F. and Elliott T. (2016)

394   High-precision mass-dependent molybdenum isotope variations in magmatic rocks determined

395   by double-spike MC-ICP-MS. Geostand. Geoanal. Res. 40, 389–403.

396   Xu L.-J., Liu S.-A. and Li S. (2021) Zinc isotopic behavior of mafic rocks during continental deep

397   subduction. Geosci. Front. 12(5) 101182.

398   Yang J., Barling J., Siebert C., Fietzke J., Stephens E. and Halliday A. N. (2017) The molybdenum

399   isotopic compositions of I-, S and A-type granitic suites. Geochim. Cosmochim. Acta 205,

400   168–186.

401   Zhang Y., Yuan C., Sun M., Li J., Long X., Jiang Y. and Huang Z. (2020) Molybdenum and boron

402   isotopic evidence for carbonrecycling via carbonate dissolution in subduction zones. Geochim.

403   Cosmochim. Acta 278, 340–352.

404   Zhao, P.-P., Li J., Zhang L., Wang Z.-B., Kong D.-X., Ma J-L., Wei G.-J., Xu j.-F.. (2015)

405   Molybdenum mass fractions and isotopic compositions of interna tional geological reference

406   materials. Geostand. Geoanal. Res. 40, 217–226.

407   Zindler A. and Hart S. (1986) Chemical geodynamics. Annu. Rev. Earth Planet. Sci. 14, 493–571.

408

Table 1 Molybdenum isotopic composition of Northeast China basalt and geological reference materials

Sample	Mo(μg g^{-1})	MgO(%)	Na$_{8.0}$	LOI	Ce/Pb	Th/U	Ba/Th	(La/Yb)$_N$	^{87}Sr/^{86}Sr	^{143}Nd/^{144}Nd	δ^{98}Mo	2SD
Keluo												
DYS12-01	2.42	7.93	3.61	0.86	10.9	4.94	239	40.6	0.70514	0.51240	-0.38	0.04
DYS12-02	2.45	7.89	3.48	0.75	9.83	5.01	224	43.7	0.70509	0.51241	-0.36	0.04
XYS12-01	2.63	8.02	4.12	0.16	8.53	5.06	147	47.7	0.70541	0.51239	-0.41	0.03
XYS12-04	2.53	8.6	3.98	0.4	17.0	5.15	176	49.1	0.70534	0.51236	-0.38	0.05
JS12-01	1.48	11.28	4.16	1.28	15.4	5.46	227	39.8	0.70511	0.51242	-0.32	0.04
JS12-02	1.52	11.3	4.25	0.9	15.2	5.40	223	36.3	0.70503	0.51243	-0.38	0.03
DZS12-02	1.46	11.43	4.90	0.08	17.6	5.52	202	41.5	0.70514	0.51243	-0.23	0.05
DZS12-03	1.32	11.62	5.09	0.06	17.0	4.93	231	44.3	0.70507	0.51246	-0.34	0.03
XGS12-01	1.73	10.11	4.04	0.68	9.26	4.96	201	42.8	0.70527	0.51238	-0.28	0.04
XGS12-02	1.88	9.93	4.02	0.34	9.99	5.87	198	43.2	0.70531	0.51238	-0.29	0.05
HS12-01	1.21	12.13	4.96	0.12	15.4	6.32	231	35.2	0.70514	0.51244	-0.34	0.04
HS12-03	1.38	12.05	5.02	0.06	20.35	6.12	238	37.2	0.70516	0.51241	-0.32	0.03
Halaha-Chaoer												
07CH02	1.04	12.97	4.64	0.10	17.40	4.13	134	10.2	0.70365	0.51293	-0.15	0.03
07AES07	1.01	10.88	4.27	0.30	12.14	4.09	105	10.3	0.70371	0.51291	-0.12	0.03
07AES09	0.96	10.43	4.13	0.12	15.59	3.98	97	9.4	0.70369	0.51293	-0.18	0.04
07AES16	1.18	12.5	4.82	0.11	20.34	4.44	109	9.9	0.70354	0.51293	-0.13	0.05
Geological reference materials												
NOD-P-1											-0.79	0.04
NOD-A-1											-0.87	0.05
BCR-2											-0.06	0.04
BHVO-2											-0.05	0.05
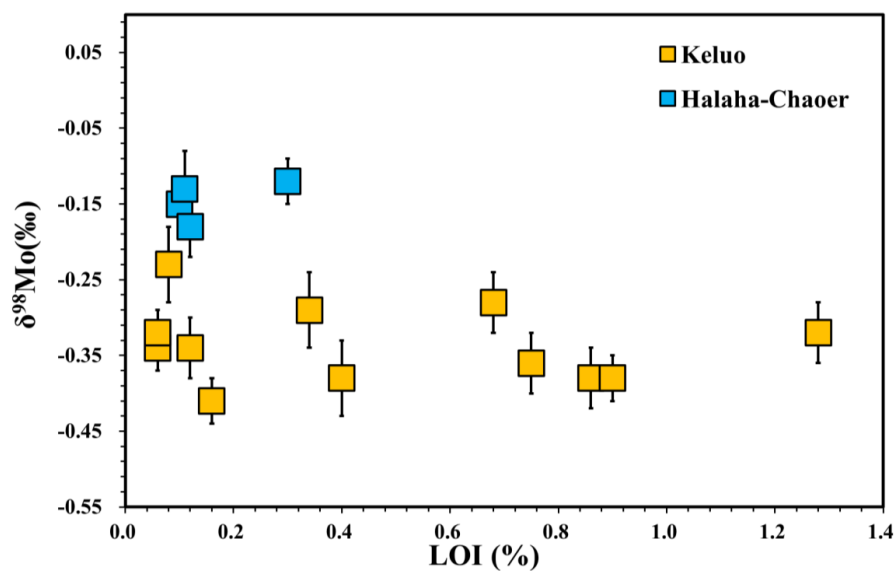
Fig.1 δ^{98}Mo versus loss on ignition (LOI) for Northeast China basalts. Data are reported in
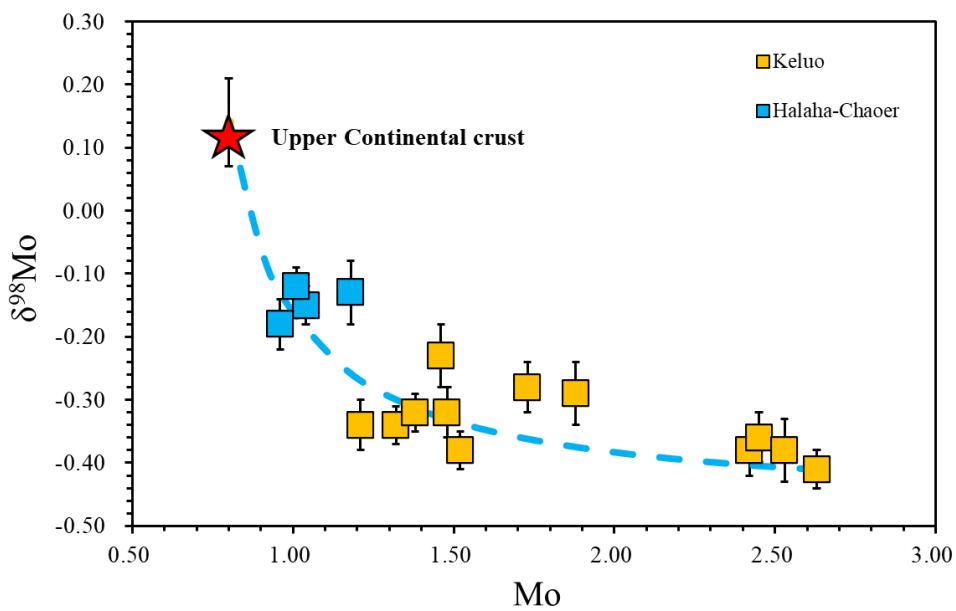
Table 1

Fig.2 Plots of δ^{98}Mo against Mo concentration for Northeast China basalts. The average Mo

isotopic composition of upper continental crust is 0.14 ± 0.07‰ (Yang et al., 2017). Data are

reported in Table 1.
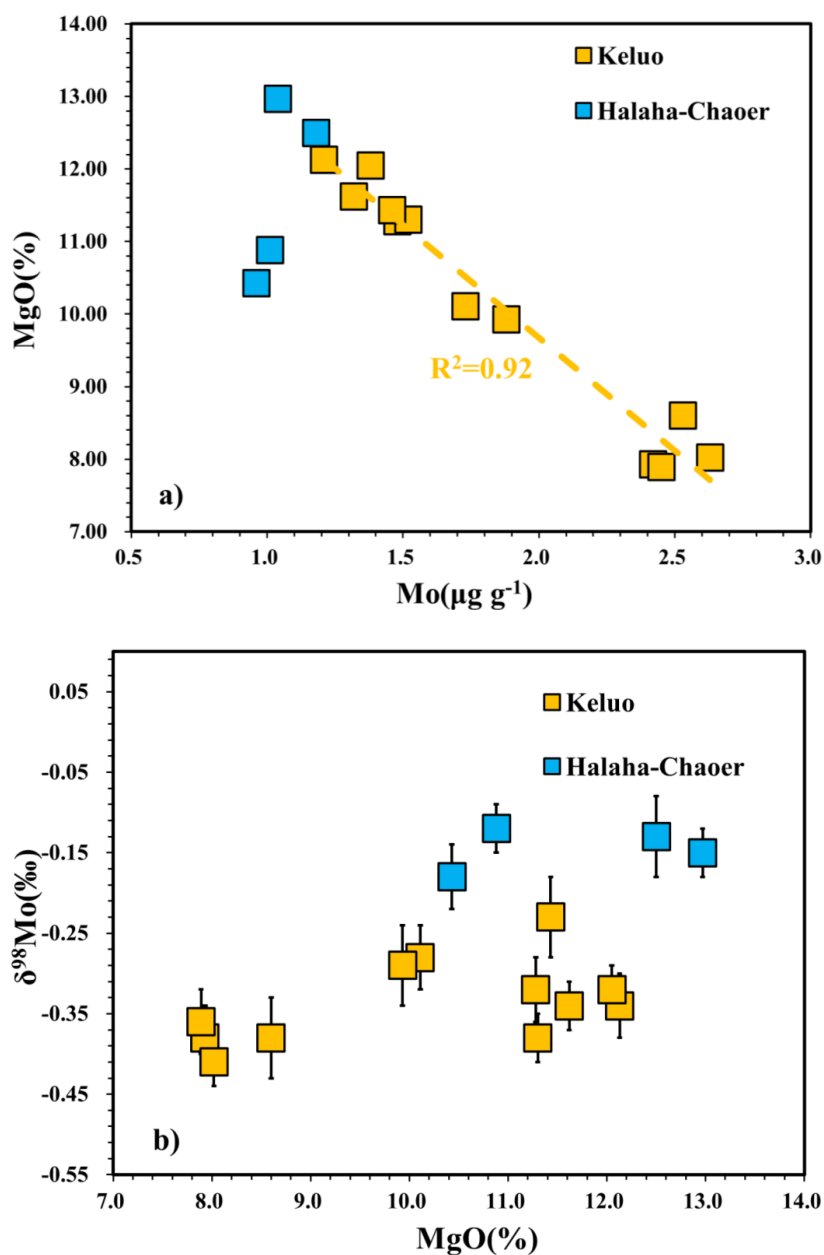
Fig. 3 Plot of δ^{98}Mo against Mo concentration (a) and MgO content (b) for Northeast China
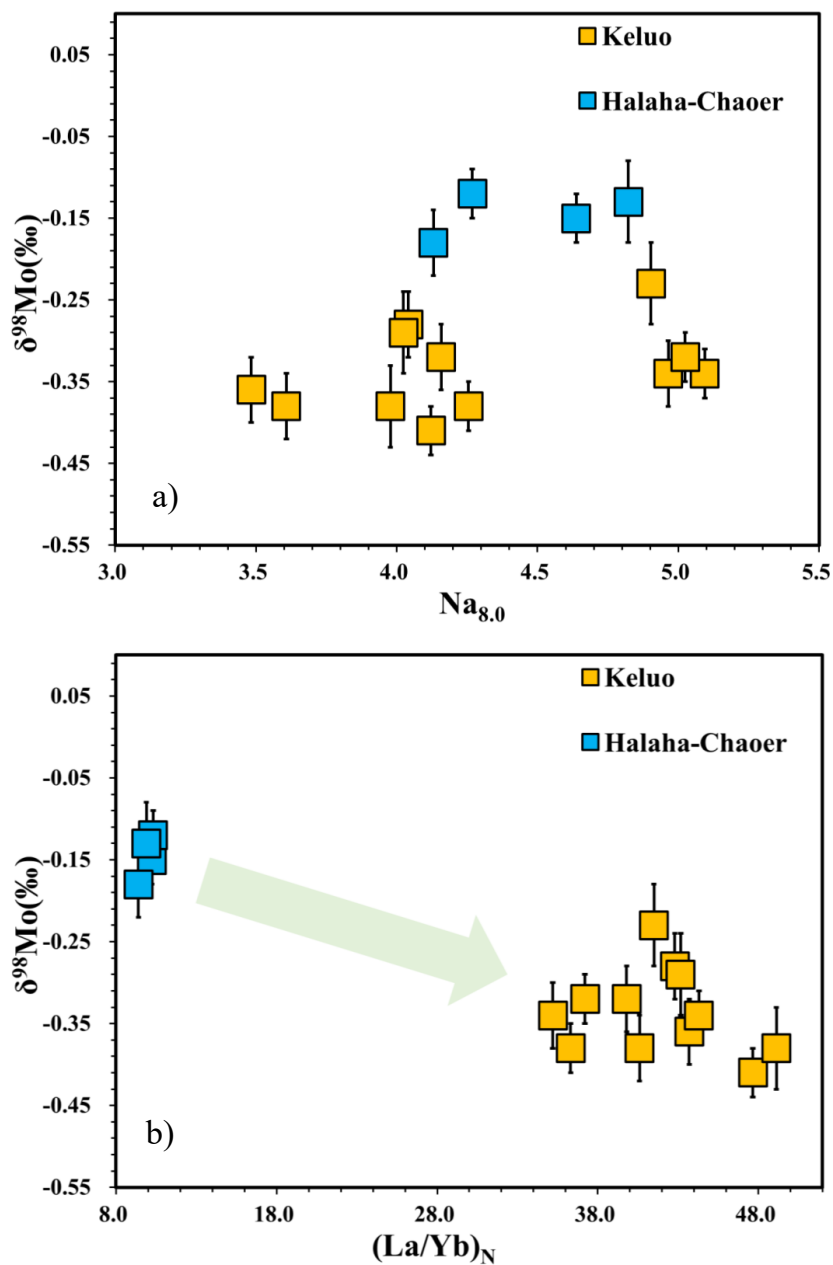
basalts.

Fig. 4 δ^{98}Mo versus Na$_{8.0}$ (a) and (La/Yb)$_N$ (b) for Northeast China basalts. Na$_{8.0}$ was

calculated by Na$_{8.0}$ = Na2O+(0.373×MgO)-2.98 (Klein and Langmuir, 1987). Data are

reported in Table 1
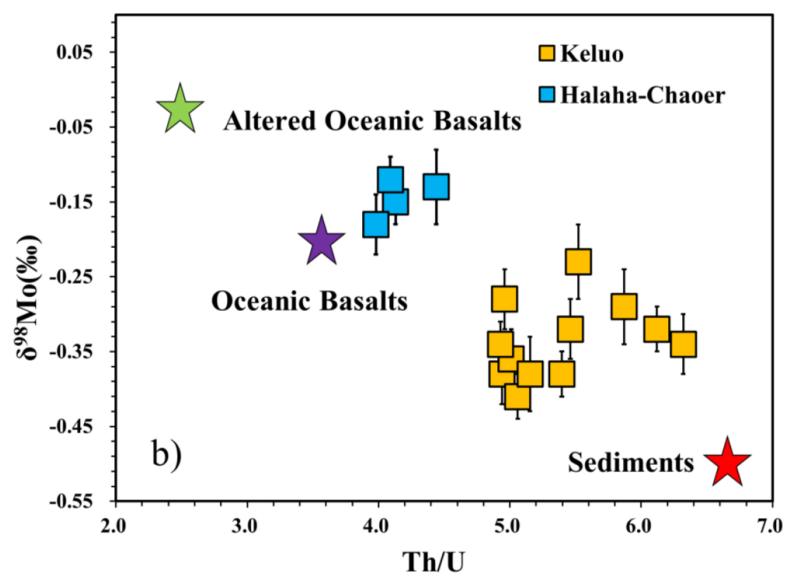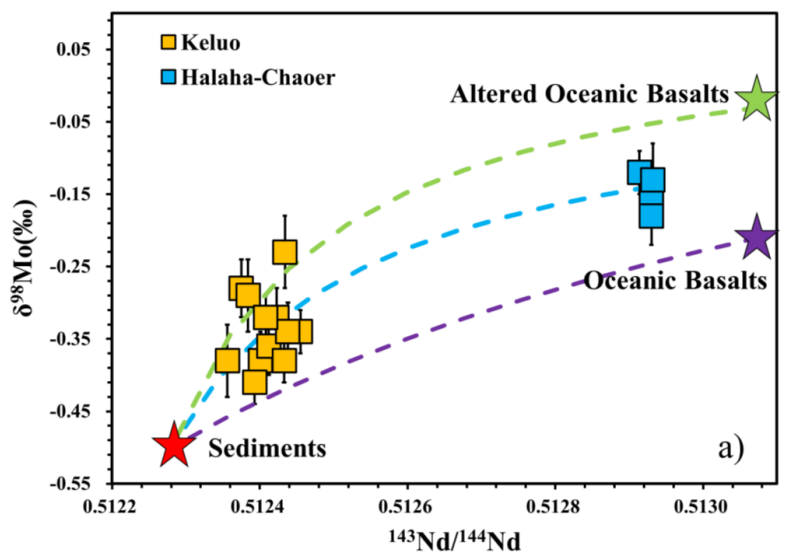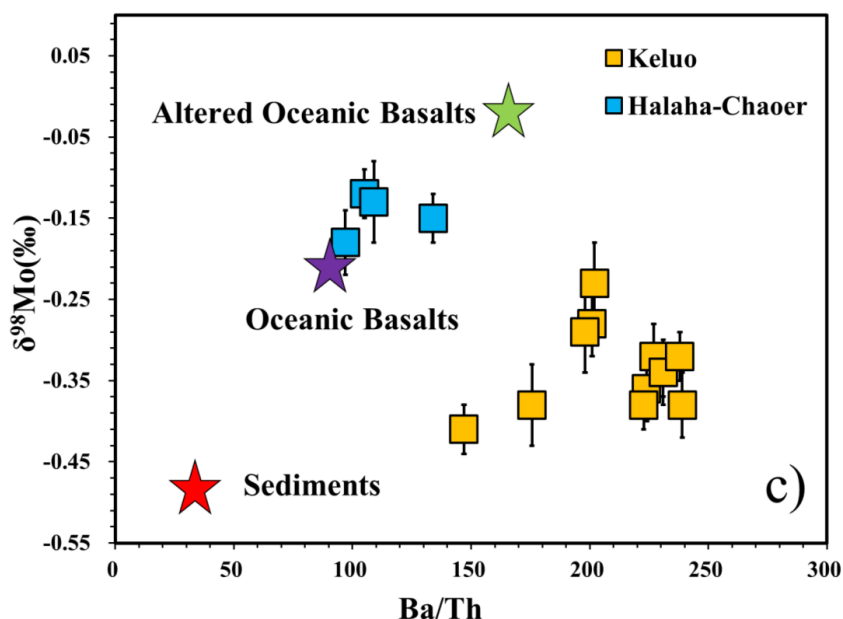
Fig. 5 Plot of δ^{98}Mo against ^{143}Nd/^{144}Nd (a), Th/U (b) and Ba/Th (C) for Northeast China

basalts. The clay-rich sediments, highly altered oceanic crust, and unaltered oceanic basalts

are represented by sediments from DSDP sites 294/295 (Vervoort et al., 2011), samples from

the Bay of Islands ophiolite (Parendo et al., 2017), and the average E-MORB (Gale et al.,

2013), respectively. The Nd isotopic ratio of clay-rich sediments is 0.512380 (Vervoort et al.,

2011), whereas the Nd isotopic compositions of highly altered oceanic crust and unaltered

oceanic basalts are assumed to be similar to that of the average E-MORB (0.513074) (Gale et

al., 2013). The Th/U and Ba/Th ratios of these components are 6.64 and 35 (Vervoort et al.,

2011), 2.5 and 166 (Parendo et al., 2017), and 3.54 and 92 (Gale et al., 2013), respectively.